Available online at www.sciencedirect.com

ScienceDirect

Proceedings of the Combustion Institute 38 (2021) 2801–2808

Proceedings of the Combustion Institute

www.elsevier.com/locate/proci

Conventional spark versus nanosecond repetitively pulsed discharge for a turbulence facilitated ignition phenomenon

M.T. Nguyen [a], S.S. Shy [a,b,*], Y.R. Chen [a], B.L. Lin [a], S.Y. Huang [a], C.C. Liu [b]

[a] *Department of Mechanical Engineering, National Central University Jhong-li District, Tao-yuan City, Taiwan*
[b] *Karlsruhe Institute of Technology, Institute of Technical Thermodynamics, Germany*

Received 8 November 2019; accepted 18 June 2020
Available online 21 July 2020

Abstract

This work applies both conventional-single-spark-discharge (CSSD) at 500-μs pulse duration time and nanosecond-repetitively-pulsed-discharge (NRPD) at various pulsed-repetitive-frequency PRF = 5–70 kHz to explore a turbulence facilitated ignition (*TFI*) phenomenon using a pair of pin-to-pin electrodes at an inter-electrode gap of 0.8 mm in randomly-stirred lean n-butane/air mixture with Lewis number ≫ 1. For CSSD, measured laminar and turbulent minimum ignition energies (MIE_L and MIE_T) at 50% ignitability show that $MIE_L \approx$ 23 mJ > the smallest $MIE_T \approx$ 19.7 mJ at $u' = 0.9$ m/s (*TFI*) and then $MIE_T \approx$ 28.6/30.8/36.8 mJ at $u' = 1.4/2.1/2.8$ m/s (no *TFI*), where u' is the r.m.s turbulent fluctuating velocity. For comparison, all NRPD experiments apply the same total ignition energy $E_{tot} \approx$ 23 mJ via a fixed train of 11 pulses, each pulse with 2.2 mJ except for the first pulse with 1 mJ. NRPD results show a cumulatively synergistic effect depending on the coherence between PRF and an inward reactant flow recirculation frequency (f_{RC}) inside the torus-like kernel induced by the discharge that could enhance ignition. When PRF is approximately synchronizing with f_{RC}, the synergistic effect is most profound at PRF = 20-kHz/40-kHz with very high ignition probability P_{ig} = 90%/85% > 50% in quiescence, whereas lower values of P_{ig} = 42%/34% are found at PRF = 10-kHz/60-kHz. Further, $P_{ig} = 0$ at PRF = 5-kHz even when 5000 pulses ($E_{tot} \approx$ 10 J) are applied. We discover that P_{ig} decreases significantly with increasing u' for most PRFs (no *TFI*) except at higher PRF ≥ 60 kHz showing possible *TFI*. These results are attributed to the interactions between turbulent dissipation, differential diffusion, and synergistic influence, which are substantiated by Schlieren images of initial kernel development and

* Corresponding author at: Department of Mechanical Engineering, National Central University Jhong-li District, Tao-yuan City, Taiwan.
E-mail address: sshy@ncu.edu.tw (S.S. Shy).

https://doi.org/10.1016/j.proci.2020.06.020

the ignition time determined at one half of the flame critical radius that leads to a self-sustained spherical flame propagation.

Keywords: Nanosecond repetitively pulsed discharge; Pulsed repetitive frequency; Turbulence facilitated ignition; Ignition probability; Turbulent dissipation; Differential diffusion

1. Introduction

How to develop reliable ignition sources for lean-burn devices with low emission is an important issue [1-3]. When using the conventional-single-spark-discharge (CSSD) ignition system (e.g., [3–9] among many others), there is a serious misfire problem in internal combustion engines under lean operating conditions. As noted by Ju and Sun [1], one of plasma-assisted discharges, namely the nanosecond-repetitively-pulsed-discharge (NRPD), is a very promising energy deposition technique for the enhancement of ignition and combustion. Recently, the NRPD technique has attracted great attention for investigation of the ignition enhancement using a pair of pin-to-pin electrodes in flows that are either in quiescence or with large mean velocity (e.g., pulsed detonation engine [10], flowing methane/air mixtures [11], 3-D DNS quiescent lean methane/air mixture [12], quiescent lean propane/air mixture using a constant-volume combustion chamber [13–16]). Based on the best knowledge of the authors, the NRPD study in near-isotropic turbulence characterized by an energy-weighted r.m.s. turbulent fluctuating velocity (u') with negligible mean velocities is still not available. This motivates the present study to explore the effect of u' on the ignition probability (P_{ig}) of NRPD over a range of pulsed repetitive frequency (PRF = 5–70 kHz). Hence, we investigate how exactly a turbulence facilitated ignition (*TFI*) phenomenon found by the CSSD ignition system using a pair of pin-to-pin electrodes would vary with a change of PRF and u'.

What is *TFI*? *TFI* means that the required ignition energy (E_{ig}) for successful ignition in turbulent conditions is smaller than that in quiescence through differential diffusion if the effective Lewis number (*Le*) of mixtures is sufficiently larger than unity, as first observed by Wu et al. [17] using CSSD with small inter-electrode gaps ($d_{gap} \leq$ 0.8 mm) in near-isotropic turbulence. Further, Saha et al. [18] reported a competing role of turbulence and differential diffusion for the occurrence and disappearance of *TFI* using CSSD at $d_{gap} = 0.8$ mm in randomly stirred n-butane/air mixture ($\emptyset = 0.7$, $Le \approx 2.2 \gg 1$). They revealed that such *TFI* phenomenon only occurs in weak and/or moderate turbulence, because strong turbulence re-asserts its dominant role and renders ignition more difficult. Note that *TFI* is very sensitive to d_{gap}. Recently, Shy et al. [3,19] measured the effect of d_{gap} on *TFI* by applying the same rich hydrogen/air mixture at $\varphi = 5.1$ with $Le \approx 2.3 \gg 1$ as in [17] in a large fan-stirred cruciform bomb capable of generating near-isotropic turbulence. Based on measured laminar and turbulent minimum ignition energies (MIE_L and MIE_T), Shy et al. [19] discovered that *TFI* only occurs at sufficiently small d_{gap} (typically < 1 mm) and at sufficiently large $Le \gg 1$, whereas *TFI* disappears when $d_{gap} > 1$ mm. Moreover, Shy et al. [3] substantiated that the occurrence of *TFI* is due to a ball-like embryonic kernel at sufficiently small d_{gap} having large positive curvature that weakens reaction rate through differential diffusion for $Le \gg 1$ making ignition much more difficult to occur in quiescence than in turbulence. No *TFI* when $d_{gap} >$ 1 mm, because the embryonic kernel is rod-like with small or negligible positive curvature (see Fig. 4c in [3]). It is thus interesting to apply the most promising NRPD ignition system [1] for investigating the aforesaid *TFI* phenomenon.

Previous NRPD studies (e.g., [10–16]) have provided important knowledge and information on the cumulative effect of successive NRPD at some certain PRFs, typically around 10–40 kHz depending on various parameters such as d_{gap}, the total deposited energy (E_{tot}), and flow conditions, showing a significant enhancement of P_{ig}. Such cumulative effect can be called as the synergistic effect, which might be attributed to the coherence between characteristic recirculation time (τ_{RC}) from the discharge-induced flow field and the inter-pulse time (PRF^{-1}) (e.g., [12–16]). In short, the present work has three objectives: (1) to explore for the first time the interactions among effects of the NRPD synergy, differential diffusion, and turbulent dissipation for possible *TFI* and ignition enhancement using the lean n-butane/air mixture at $\varphi = 0.7$ with $Le \approx 2.2 \gg 1$ and $d_{gap} = 0.8$ mm as that used in [18]; (2) to measure MIE_L and MIE_T over a range of u' for the same mixture and d_{gap} as in (1) using CSSD; and (3) to gain a better understanding of laminar and turbulent ignition characteristics between NRPD and CSSD.

2. Experimental methods

Both CSSD and NRPD ignition experiments of the n-butane/air mixture at $\varphi = 0.7$ with $Le \approx 2.1 \gg 1$ were conducted in a large dual-chamber fan-stirred cruciform explosion facility using the same 2-mm stainless steel electrodes with sharp ends at a fixed $d_{gap} = 0.8$ mm which are cantilevered at an angle of 45° to the horizon and positioned at the center of the experimentation domain. The averaged minimum diameter inside the large fan-stirred cruciform burner was about 30 cm. The burner was equipped with a pair of counter-rotating fans and perforated plates capable of generating near-isotropic turbulence within a region of $15 \times 15 \times 15$ cm^3. The reader is directed to Ref. [3] and references therein for detailed information on the explosion facility, associated turbulence properties, and mixture preparation before ignition, so they are not elaborated upon here. The followings are the descriptions on how to measure CSSD and NRPD ignition energies (E_{ig}) in the present study.

Since the spark breakdown is statistical in nature, it is necessary to measure E_{ig} in situ directly from the discharged electrodes. For CSSD, we apply a precision high-voltage pulse generator with a maximum breakdown voltage of 25 kV (HV-M25K) together with adjustable loading resistances and a small damping resistor of 100 Ω in a home-made ignition circuit to create near-square voltage and current waveforms within the selected pulse duration time varying from 1 μs to a few milliseconds, same as that used in our previous MIE transition studies [20]. As shown in Fig. 1(a) as a typical example, accurate $E_{ig} = 23.2$ mJ can be measured by the integration of the product of the discharged current $I(t)$ and the voltage difference $[V_1(t) - V_2(t)]$ across the spark gap between electrodes within $\tau_p = t_2 - t_1$ (= 500 μs), where the breakdown voltage used is 15 kV and the discharged voltages and current are measured by two high-voltage Tektronix probes and the Pearson current probe [20]. In an attempt to make a comparison between CSSD and NRPD ignition characteristics, we first measure the value of MIE_L for the lean n-butane/air mixture ($\varphi = 0.7$) at $d_{gap} = 0.8$ mm and $\tau_p = 500$ μs in quiescence. MIE is a statistical property, not a threshold value, because there is an overlapping regime of E_{ig} within which "Go" and "No Go" ignition events coexist at the same E_{ig}. In the Supplemental Materials, Fig. S1 shows that $MIE_L = 22.7$ mJ at 50% ignitability using the logistic regression method. Each value of MIE_L and MIE_T determined at 50% ignitability is obtained from 20∼40 trials over a range of well-controlled E_{ig}. Note that the same cantilevered electrodes with sharp ends, as indicated in Fig. 1(a), are applied for both CSSD and NRPD experiments.

As to the NRPD study, the power supply (FID GmbH FPG 20–100NK) produces peak pulse amplitudes up to 30 kV, pulse durations of 3–5 ns FWHM, and pulsed repetitive frequencies up to 100 kHz. A delay/pulse function generator (GW INSTEK AFG-2225) is used to control the NRPD power supply via external trigger signals. For all NRPD ignition experiments, we apply a fixed peak open-circuit voltage of 28 kV over a range of PRF = 5–70 kHz with a burst of 11 pulses having a constant total ignition energy $E_{tot} \approx 23$ mJ which is almost the same as $MIE_L = 22.7$ mJ measured by CSSD. The NRPD voltage and current signals are respectively measured by high voltage probe (Tektronix P6015A) and Pearson coil (model 6585), which are recorded by a 500 MHz oscilloscope (Tektronix MD03054). Fig. 1(b) shows voltage, current, and energy waveforms of the second pulse from a burst of 11 pulses at PRF = 20 kHz, as a typical example for single nanosecond-pulse discharge. As seen from Fig. 1(b), after the first major voltage/current peak, oscillating voltage/current waves can be observed which contribute to a small portion of the integrated discharge energy. Note that the wave profile remains roughly the same for each nanosecond-pulse. Fig. 1(c) displays all 11 NRPD voltage and current signals at PRF = 20 kHz with $E_{tot} \approx 23$ mJ. Fig. 1(d) presents the accumulated energy depositions plotted against the pulse number from the burst of 11 pulses which are nearly the same at different PRFs = 10–60 kHz. The individual energy of each pulse from the burst of 11 pulses is about 2.2 mJ, independent of the PRF, except for the first pulse having a lower E_{ig} of about 1 mJ, similar to that reported in [11]. Moreover, Schlieren images of initial kernel development for both CSSD and NRPD are recorded by a high-speed, high-resolution camera (Phantom V711) at 10,000 frames/s with 800 × 800 pixels.

3. Results and discussions

3.1. Ignition probability and kernel development in quiescence

Ignition is statistical in nature. A successful ignition event (Go) must include all three stages from the breakdown and the formation of flame kernel to the self-sustained propagation flame. If only the breakdown and the kernel formation occur without the development of self-sustained propagation flame, this event belongs to failure ignition (No Go). The NRPD ignition probability (P_{ig}) is defined as the ratio of the number of successful ignitions to the total number of ignition trials. Thus, many ignition trials are required to obtain an accurate P_{ig}. Fig. 2 shows laminar $P_{ig,L}$ versus the number of cumulative trials for six different PRFs = 5-kHz/10-kHz/20-kHz/40-kHz/60-kHz/70-kHz corresponding to $P_{ig,L}$ = 0%/42%/90%/85%/34%/27%,

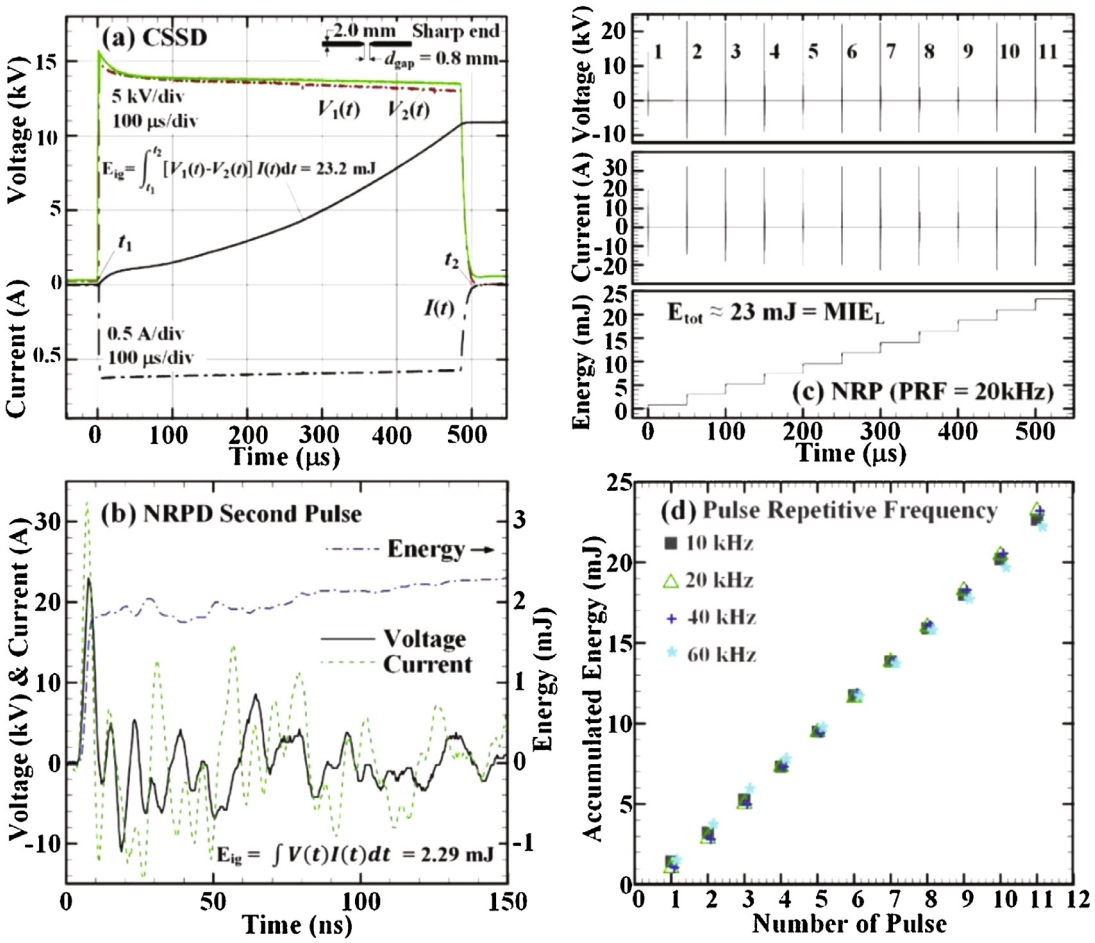

Fig. 1. The same pin-to-pin electrodes at $d_{gap} = 0.8$-mm are used for both CSSD and NRPD. (a) Typical CSSD's square-waveforms of voltage, current, and E_{ig} at $\tau_p = 500$ μs. (b) Typical NRDP's voltage, current, and energy waveforms for the second pulse from a burst of 11 pulses taken at 20 kHz. (c) Same as (b), but for all 11 pulses. (d) Accumulated energy deposition of 11 pulses at different PRFs, where $E_{tot} \approx 23$ mJ for all PRFs.

using a fixed train of 11 pulses with $E_{tot} \approx 23$ mJ $\approx MIE_L$. In this study, 60 trials are used to obtain a reliable value of P_{ig} at each of different PRFs (Fig. 2). At $d_{gap} = 0.8$ mm, the highest $P_{ig,L} = 90\%$ occurs at PRF = 20 kHz. If the smaller number of pulse than 11 pulses is used, $P_{ig,L}$ decreases. On the other hand, $P_{ig,L}$ increases if the pulse number increases. Please see Fig. S2 in the Supplemental Materials, where the effect of pulse number on P_{ig} is demonstrated using PRF = 20 kHz, as a typical example. To better explain and understand why the non-monotonic increase and decrease of P_{ig} with the maximum $P_{ig} = 90\%$ at PRF = 20 kHz happen, we examine the early development of the embryonic kernel at various PRFs.

Fig. 3 shows Schlieren images of ignition kernel structures and their subsequent flame development in quiescence for four different cases, including (a) a CSSD case at $\tau_p = 0.5$ ms and (b) three NRPD cases at PRF = 5 kHz, 20 kHz, and 60 kHz, respectively. These four different cases apply the same $E_{ig} \approx 23$ mJ ($\approx E_{tot}$), lean n-butane/air with $Le \approx 2.2 \gg 1$, and $d_{gap} = 0.8$ mm < 1 mm. In Fig. 3, the first four columns have a smaller view field of 16×16 mm^2 to see the embryonic kernel, while the fifth column has a larger view field of 42×42 mm^2 to view self-sustained flame propagation. There are three key points. First, the CSSD case (Fig. 3a) has a $P_{ig} = 50\%$, where $MIE_L \approx 22.7$ mJ when using $Le \approx 2.2 \gg 1$ mixture at $d_{gap} = 0.8$ mm. This is due to the fact that the large positive curvature of the embryonical kernel at 0.1 ms (the first image of Fig. 3a having a torus-like shape) weakens reaction rate through differential diffusion (also see

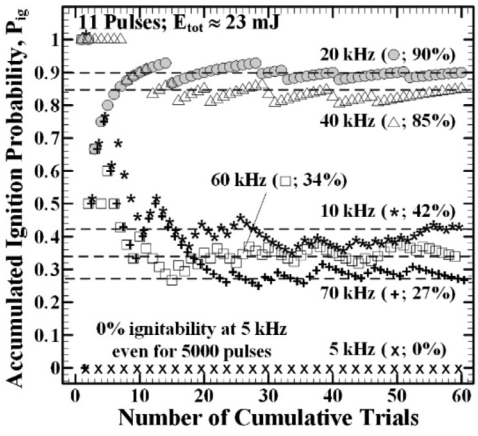

Fig. 2. The NRPD ignition probability versus the number of cumulative trials at different PRFs.

Fig. 4c of Ref. [3]). Note that there is no wrinkling inside the single-shot CSSD torus-like (elliptic) embryonic kernel at 0.1 ms and 0.5 ms. Second, at PRF = 5 kHz (the first row of Fig. 3b), all 60 ignition trials never ignite successfully at $E_{tot} \approx 23$ mJ (see also Fig. 2). Although the first embryonic hot kernel ignited by the first pulse of only about 1 mJ (the first image at 0.1 ms) looks just like the CSSD kernel at 0.1 ms (Fig. 3a), it is cooled down by the inward recirculation flow induced by the discharge. This is because the inter-pulse time of 200 μs (PRF = 5 kHz) is too long as compared to the typical timescale of flow recirculation, resulting in a fade-out before the arrival of the second pulse at 0.5 ms (no synergistic effect). Such cool-down and fade-out processes continue to the tenth pulse at 2 ms and to the last pulse at 2.2 ms (not shown), leading to failure ignition (No Go). Could an increase of pulses (more than 11 pulses) at PRF = 5 kHz result in a successful ignition? The answer is no. We discover that even applying 5000 pulses with $E_{tot} = 10$ J, P_{ig} remains zero at PRF = 5 kHz. Third, at PRF = 20 kHz (the second row of Fig. 3b), $P_{ig} = 90\% \gg P_{ig} = 50\%$ for the CSSD case. There are strong wrinkling structures inside the embryonic torus-like hot kernel due to the superadded multiple pulses, as can be clearly seen from the first and second images at 0.1 ms and 0.5 ms, showing the strongest synergistic effect that enhances significantly the P_{ig} when using the present electrode configuration. It is anticipated that the synergistic effect is most profound when the inter-pulse time is approximately synchronizing with τ_{RC}, implying that τ_{RC} is roughly on the order of 50 μs (~ 20 kHz) in the present setup. The early developing stage of the aforesaid strongest synergistic kernel is accelerated by superadded mul-

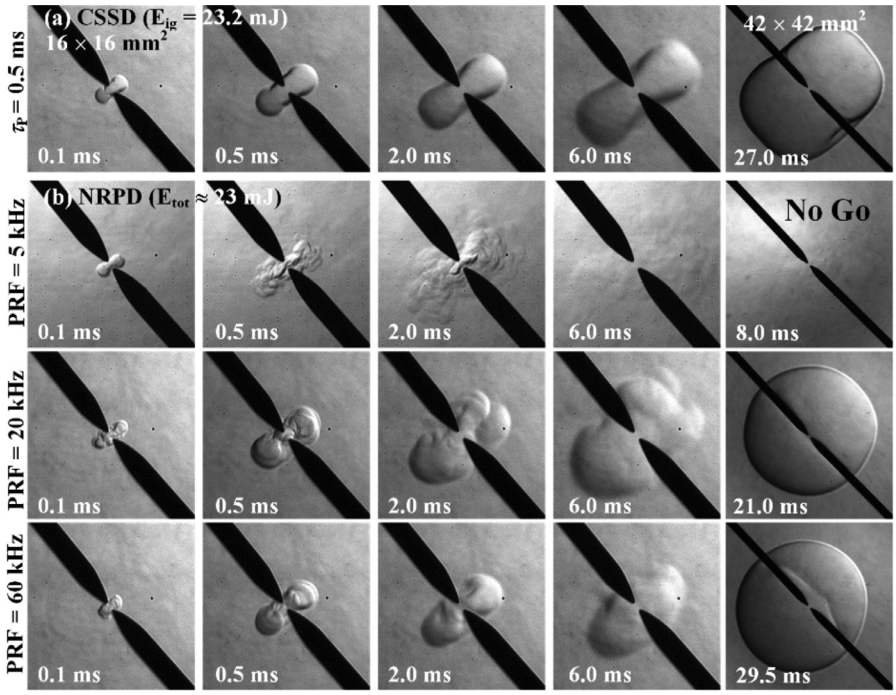

Fig. 3. Development of ignition kernel to self-sustained flame propagation in quiescence: (a) CSSD at $\tau_p = 500$ μs and (b) NRPD with a fixed train of 11 pulses at three PRFs = 5, 20, 60 kHz, using the same $E_{ig} \approx E_{tot} \approx 23$ mJ in the same lean n-butane/air mixture at the same $d_{gap} = 0.8$ mm.

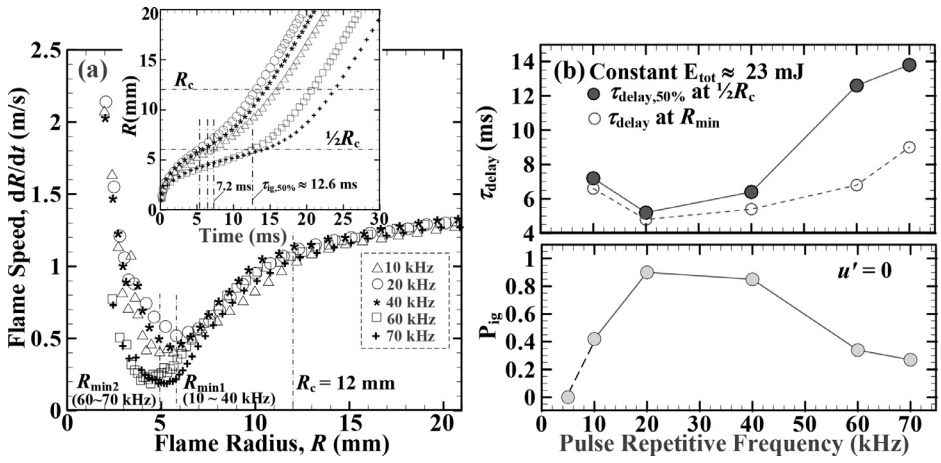

Fig. 4. (a) Flame speed plotted against flame radius at five different PRFs using the same experimental settings, which are obtained from the raw flame radii versus time (the inset figure). (b) The ignition delay time (τ_{delay}) as a function of PRF, where two kinds of τ_{delay} at R_{min} and R_c are estimated from (a). Also plotted is the ignition probability (P_{ig}) as a function of PRF using the same $E_{tot} \approx 23$ mJ $\approx MIE_L$ (E_{ig} at 50% ignitability for the CSSD case).

tiple pulses, where the wrinkled flame kernel with locally negative and positive curvature stretch can be observed at 2 ms and 6 ms images in the second row of Fig. 3b. Such wrinkled kernel soon develops into a self-sustained propagating spherical flame (see the image at 21 ms). The situation at PRF = 60 kHz (the third row of Fig. 3b) is similar to that at PRF = 20 kHz, but having a much weaker synergistic effect where $P_{ig} = 34\% < P_{ig} = 50\%$ for the CSSD case.

3.2. Ignition delay time as a function of PRF

To quantify the ignition delay time as a function of pulsed repetitive frequency for successful ignition, we record the time evolutions of flame kernel radii (R) using high-speed Schlieren imaging (see Fig. 3b), where $R = (A/\pi)^{0.5}$ and A is the area enclosed by the flame front. As such, flame speeds (dR/dt) versus R can be obtained. Fig. 4(a) presents five data sets of dR/dt vs. R at five different PRFs = 10, 20, 40, 60, 70 kHz. All five flame speeds on the burned side ($S_L{}^b$) first decrease drastically and then reach their minimum ($S_L{}^b{}_{min}$) at corresponding radii (R_{min}) depending on PRF for the lean n-butane/air mixture with $Le \approx 2.2 \gg 1$. These $R(S_L{}^b{}_{min})$ data can be divided into two groups: (1) $R_{min1} \approx 6$ mm covering PRF = 10, 20 and 40 kHz with higher values of $S_L{}^b{}_{min}$ and (2) $R_{min2} \approx 5$ mm for PRF = 60 and 70 kHz with lower values of $S_L{}^b{}_{min}$. Then all five dR/dt data increase and merge together at a critical flame radius $R_c \approx 12$ mm to approach the planar value which is independent of PRF. The inset in Fig. 4(a) presents the raw data of $R(t)$ vs. t at five PRFs varying from 10 kHz to 70 kHz, demonstrating again that the times required to reach R_c from the fastest to the slowest are in sequence of 20 kHz, 40 kHz, 10 kHz, 60 kHz, and 70 kHz. Also, the slopes of these five PRF data beyond R_c are the same, indicating the flame speed is constant, regardless of PRF at least within the range of 10–70 kHz. Two ignition delay times are estimated, one located at $0.5R_c$ ($\tau_{delay,50\%Rc}$) and the other located at R_{min} ($\tau_{delay,Rmin}$) where the flame speed is the lowest. As shown on the top of Fig. 4(b), we find that $\tau_{delay,50\%Rc}$ is only slightly higher than $\tau_{delay,Rmin}$ within 10–40 kHz, but $\tau_{delay,50\%Rc}$ is much higher than $\tau_{delay,Rmin}$ at 60 kHz and 70 kHz. Since the ignition delay time is inversely proportional to the ignition probability, the ignition delay time determined at one half of the flame critical radius should be a better representing parameter as its non-monotonic curve fits inversely better with that of $P_{ig,L}$ (see the bottom of Fig. 4b). Specifically, $\tau_{delay,50\%Rc} = 5.2$ ms (20 kHz) and 6.4 ms (40 kHz) corresponding to $P_{ig,L} = 90\%$ and 85%, whereas $\tau_{delay,50\%Rc} = 7.2$ ms (10 kHz), 12.6 ms (60 kHz), and 13.8 ms (70 kHz) corresponding to $P_{ig,L} = 42\%$, 34%, and 27%. Based on the results of $\tau_{delay,50\%Rc}$ using the same $E_{tot} \approx 23$ mJ, it is concluded that the synergistic effect is most obvious at 20–40 kHz having very high $P_{ig,L} \gg 50\%$, while lower and higher PRFs become detrimental for ignition having lower $P_{ig,L} < 50\%$.

3.3. CSSD and NRPD ignition characteristics in near-isotropic turbulence

Fig. 5 shows the effect of u' on P_{ig} and/or MIE for both NRPD and CSSD cases alongside the evolutions of Schlieren kernels at PRF = 60 kHz with three different $u' = 0$, 0.5, and 0.9 m/s on the right part of the figure. The inset in Fig. 5 is for

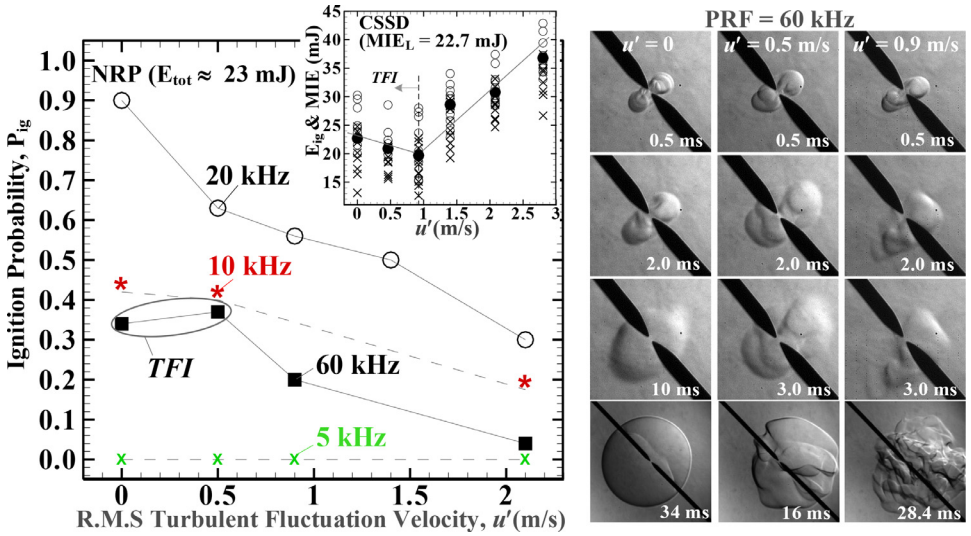

Fig. 5. Left: The NRPD's P_{ig} plotted against u' at four different PRFs using a constant $E_{tot} \approx 23$ mJ via a fixed train of 11 pulses. The inset is for the CSSD case at $\tau_p = 500$ μs, showing a non-monotonic decrease and increase of MIE with increasing u' where $MIE_L = 22.7$ mJ > $MIE_T = 19$ mJ at $u' = 0.9$ m/s (*TFI*). Right: Three Schlieren kernel development image sets in quiescence and turbulence conditions at PRF = 60 kHz with three different $u' = 0$, 0.5, and 0.9 m/s having a small view field of 16 × 16 mm^2. Images at the last row have a large view field of 60 × 60 mm^2.

the CSSD case, in which all MIE data (black circle symbol) are measured at $\tau_p = 500$ μs and determined at 50% ignitability with successful ignition (open circle symbol) and failure ignition (cross symbol). A non-monotonic decrease and increase of MIE with increasing u' is found in support of the finding of Saha et al. [18], although the present values of MIE_L and MIE_T are much smaller than that reported in [18] who measured MIE at an ignition probability higher than 50%. Note that the lowest MIE ≈ 19 mJ occurs at u' ≈ 0.9 m/s, suggesting that there is *TFI* when u' < 0.9 m/s where $MIE_T < MIE_L = 22.7$ mJ. However, when $u' > 0.9$ m/s, turbulence regains its dominance where MIE_T (> MIE_L) increases with increasing u'. As to the NRPD case, four data sets of $P_{ig,L}$ and $P_{ig,T}$ at PRF = 5, 10, 20 and 60 kHz are plotted against u' for clarity, where the subscripts L and T represent laminar and turbulent conditions. We discover that $P_{ig,T}$ decreases significantly with increasing u' for most PRFs (no *TFI*), except at higher PRF = 60 kHz where $P_{ig,T} = 37\%$ at $u' = 0.5$ m/s > $P_{ig,L} = 34\%$ at $u' = 0$ showing *TFI*. At any given u', $P_{ig,T}$ at 20 kHz is always the highest among all PRFs studied in the present work. This is again attributed to the synergistic effect when the inter-pulse time is approximately synchronizing with the inward reactant flow recirculation time. At PRF = 60 kHz, the inter-pulse time is only 17 μs which is much shorter than the inward reactant flow recirculation time (assuming on the order of 50 μs for PRF = 20 kHz). As such, only a small amount of fresh reactant enters the inter-electrode gap between two consecutive pulses and thus the subsequent pulses mainly add ignition energy into radicals or possibly other active species, revealing a rather weak synergistic effect with a lower $P_{ig,L} = 34\%$ in quiescence (see the first column images in Fig. 5). When $u' = 0.5$ m/s, the weak and/or modest turbulence wrinkles the kernel, as seen in the second column image at 0.5 ms, generating locally negative curvature stretch that can enhance reaction rate through differential diffusion and increase $P_{ig,T} = 37\%$ (*TFI*). When $u' = 0.9$ m/s, local quench can occur, as seen by comparing the third column images at 2 ms and 3 ms, resulting in a significant drop of $P_{ig,T} = 20\%$. When $u' = 2.1$ m/s, $P_{ig,T}$ is nearly zero, showing a dominating influence of intense turbulence that renders ignition much more difficult to occur.

4. Conclusions

Using the lean n-butane/air mixture with $Le \gg 1$ and $d_{gap} = 0.8$ mm, we apply both CSSD and NRPD to explore how exactly P_{ig} and *TFI* would vary with changes of u' and PRF. For CSSD results, a non-monotonic decrease and increase of MIE with increasing u' is found, of which $MIE_L \approx 23$ mJ > $MIE_T \approx 19$ mJ at $u' = 0.9$ m/s, showing *TFI*. But turbulence re-claims its dominating role when $u' > 0.9$ m/s where $MIE_T > MIE_L$.

As to NRPD studies using a fixed train of 11 pulses with $E_{tot} \approx 23$ mJ, we discover that $P_{ig,L}$ and $P_{ig,T}$ remain zero at 5 kHz, regardless

of the pulse number (up to 5000 pulses) and u'. This is attributed to lack of synergistic effect at 5 kHz, large heat losses to electrodes at $d_{gap} = 0.8$ mm, and differential diffusion effect (positive curvature weakens reaction rate for $Le \gg 1$). The highest values of $P_{ig,L} = 90\%/85\%$ occur at PRFs = 20/40 kHz, respectively. Outside this PRF range, $P_{ig,L}$ is smaller than 50%. Such non-monotonic increase and decrease of $P_{ig,L}$ with increasing PRF is attributed to the cumulatively synergistic effect, which is most profound when the inter-pulse time ($PRF^{-1} = 50$ μs at 20 kHz) is approximately synchronizing with the inward reactant flow recirculation time. The ignition delay time determined at one half of the flame critical radius should be a better representing parameter as its non-monotonic curve fits inversely better with that of $P_{ig,L}$. Finally, $P_{ig,T}$ decreases significantly with increasing u' for most PRFs (no *TFI*), except at higher PRF ≥ 60 kHz showing possible *TFI*.

These results are important to turbulent premixed ignition, which should deserve to disseminate in our combustion community for stimulating further research. For future NRPD studies, we will measure the effect of d_{gap} on turbulent ignition characteristics as well as turbulent flame propagation behavior for $Le \gg 1$ flames.

Declaration of Competing Interest

None.

Acknowledgments

The financial support from the Ministry of Science and Technology, Taiwan, under grants (MOST 106-2923-E-008-004-MY3; MOST 106-2221-E-008-054-MY3) is greatly appreciated.

Supplementary materials

Supplementary material associated with this article can be found, in the online version, at doi:10.1016/j.proci.2020.06.020.

References

[1] Y. Ju, W. Sun, *Prog. Energy Combust. Sci.* 48 (2015) 21–83.
[2] A. Starikovskiy, N. Aleksandrov, *Prog. Energy Combust. Sci.* 39 (2013) 61–110.
[3] S.S. Shy, M.T. Nguyen, S.Y. Huang, *Combust. Flame* 205 (2019) 371–377.
[4] R.D. Reitz, *Combust. Flame* 160 (2013) 1–8.
[5] G.F.W. Ziegler, E.P. Wagner, R.R. Maly, *Symp. Int. Combust.* 20 (1985) 1817–1824.
[6] M. Kono, K. Hatori, K. Iinuma, *Symp. Int. Combust.* 20 (1985) 133–140.
[7] D. Bradley, F.K.K. Lung, *Combust. Flame* 69 (1987) 71–93.
[8] Y. Ko, R.W. Anderson, V.S. Arpaci, *Combust. Flame* 83 (1991) 75–87.
[9] T. Kravchik, E. Sher, J.B. Heywood, *Combust. Sci. Technol.* 108 (1995) 1–30.
[10] J.K. Lefkowitz, P. Guo, T. Ombrello, S.H. Won, et al., *Combust. Flame* 162 (2015) 2496–2507.
[11] J.K. Lefkowitz, T. Ombrello, *Combust. Flame* 180 (2017) 136–147.
[12] M. Castela, S. Stepanyan, B. Fiorina, A. Coussement, et al., *Proc. Combust. Inst.* 36 (2017) 4095–4103.
[13] S.V. Pancheshnyi, D.A. Lacoste, A. Bourdon, C.O. Laux, *IEEE Trans. Plasma Sci.* 34 (2006) 2478–2487.
[14] D.A. Xu, D.A. Lacoste, C.O. Laux, *Plasma Chem. Plasma Procees.* 36 (2016) 309–327.
[15] S. Lovascio, T. Ombrello, J. Hayashi, S. Stepanyan, et al., *Proc. Combust. Inst.* 36 (2017) 4079–4086.
[16] S. Lovascio, J. Hayashi, S. Stepanyan, G.D. Stancu, C.O. Laux, *Proc. Combust. Inst.* 37 (2019) 5553–5560.
[17] F. Wu, A. Saha, S. Chaudhuri, C.K. Law, *Phys. Rev. Lett.* 113 (2014) 024503.
[18] A. Saha, S. Yang, C.K. Law, *Proc. Combust. Inst.* 37 (2019) 2383–2390.
[19] S.S. Shy, M.T. Nguyen, S.-.Y. Huang, C.-.C. Liu, *Combust. Flame* 185 (2017) 1–3.
[20] L.J. Jiang, S.S. Shy, M.T. Nguyen, S.Y. Huang, D.W. Yu, *Combust. Flame* 187 (2018) 87–95.